Lattice misfit versus performance of thin film electroluminescent structures

E. A. Mastio,[a] W. M. Cranton, and C. B. Thomas
Department of Electrical and Electronic Engineering, The Nottingham Trent University, Burton Street, Nottingham NG1 4BU, England

(Received 23 June 2000; accepted for publication 31 October 2000)

Thin polycrystalline electroluminescent thin films (TFEL) of ZnS:Mn (phosphor) and Y_2O_3 (insulator) were deposited individually or as multilayers onto Si (100) substrates. Their crystallinity and the luminescent efficiency of the phosphor films were investigated at varying thermal annealing temperatures. It is shown that the luminescent quality of the phosphor layer increases up to 700 °C, whereas the electroluminescence operating intensity of TFEL devices saturates at 500 °C. The structural analysis of the insulating and phosphor layers shows that they recrystallize at annealing temperatures of, respectively, 500 and 600 °C, and that their lattice misfit doubles at processing temperatures $>=500$ °C. Since TFEL devices should benefit from enhanced luminescence efficiency and crystallinity at high annealing temperatures, we suggest that the lack of improvement in device performance beyond 500 °C is due to interface alterations. According to previous works, we propose that the lattice misfit increase between the phosphor and dielectric thin films modifies the morphology of the phosphor–insulator boundary inducing a modification of the interface states density, and hence, modifying high field electron transport properties of TFEL devices. © *2001 American Institute of Physics.* [DOI: 10.1063/1.1335646]

I. INTRODUCTION

In the field of flat panel display technology, thin film electroluminescence (TFEL) continues to provide the solution for applications requiring a rugged, high contrast display screen with wide viewing angle and a large temperature operating range.[1] TFEL displays are all solid state structures based on the device first demonstrated by Sharp in 1974,[2] and typically consist of a thin film phosphor layer sandwiched between dielectric thin films, with a transparent electrode and glass substrate allowing the internally generated light to be viewed by the user. More recently, our research group developed a TFEL device that utilizes a silicon substrate and reflecting microstructures to redirect light confined within the phosphor layer.[3] For both types of display devices, the physics of light generation via high field electroluminescence is the same, and both typically require an annealing process following deposition. This annealing process is generally accepted to increase the device performance for reasons such as improved luminescence efficiency and crystallinity of the phosphor layer. However, at annealing temperatures of ~500 °C, no major improvements are reported using conventional TFEL devices and it is the aim of this article to investigate the structural limitations resulting from high anneals.

While much material science studies have been reported on the effect of deposition temperature[4–7] and thermal annealing[8–10] upon the phosphor thin film, there has been little emphasis upon the phosphor–insulator electronic interface. The few research groups who discussed thermal annealing effects in terms of charge carrier density, suggested that a density modification of interfacial energy states is responsible for device performance saturation at annealing temperatures $>=500$ °C.[11–13] However, no work has been dedicated to the structural modifications of the electronic interface following thermal treatment. In the present work, we analyze the phosphor–insulator boundary in terms of lattice misfit in an attempt to explain the modifications in electro-optical performance that result at annealing temperatures $>=500$ °C. We present results of x-ray diffraction (XRD), photoluminescence (PL), and electroluminescence (EL) analyses of TFEL structures at varying thermal annealing temperatures.

II. EXPERIMENT

A. Thin film deposition and thermal annealing

Insulating (Y_2O_3) and phosphor (ZnS:Mn) layers of TFEL devices were individually or sequentially deposited onto rotating 4 in. silicon wafers, using radio-frequency magnetron sputtering in argon atmosphere. During the growing processes, the substrate temperature and argon pressure were kept constant at 200 °C and 3 mTorr, respectively. On-line thickness control of the various films was ensured by an interferometric recording system.[14] Postdeposition thermal annealing was performed in vacuum (1×10^{-7} Torr) on cleaved samples for 1 h. It is assumed that the as-grown films are annealed at a temperature of 200 °C, i.e., the substrate temperature during growth. The Mn concentration of the material used for the phosphor sputtering is 0.45 wt %, i.e., $\sim2.45\times10^{20}$ ions/cm^3.

The various depositions and annealing characteristics of the samples used in this work are listed in Table I. Samples NTU228 and NTU398 are, respectively, 800 nm of ZnS:Mn and 100 nm of Y_2O_3 single layers deposited on Si. These

[a]Author to whom correspondence should be addressed; electronic mail: emmanuel_mastio@yahoo.com

TABLE I. Deposition and thermal annealing conditions used for the present study. All structures deposited by radio-frequency sputtering onto Si (100) substrates.

Reference	Structure	Annealing temperature (°C)
NTU228	800 nm ZnS:Mn	200, 400, 500, 600, 700
NTU398	100 nm Y_2O_3	500
NTU259	300 nm Y_2O_3/800 nm ZnS:Mn	200, 300, 400, 500, 600
NTU161	300 nm Y_2O_3/800 nm ZnS:Mn/300 nm Y_2O_3	400, 500, 600, 700

samples enabled the separate structural analysis of the two materials composing the TFEL devices grown in our laboratory. Samples NTU259 are composed of the two first layers of our basic TFEL devices, i.e., multilayers of ZnS:Mn (800 nm) and Y_2O_3 (300 nm) deposited on Si, allowing a simultaneous study of their crystallinity and lattice dependence on thermal annealing temperature. Samples NTU161 are fully fabricated TFEL devices used for photoluminescence and electroluminescence analyses at varying thermal annealing temperatures.

B. X-ray diffraction, electroluminescence, and photoluminescence measurements

XRD analyses were performed to investigate the crystallinity of the samples NTU228, NTU398, and NTU259, using reflections from the Cu $K\alpha_1$ emission line (wavelength $=0.154\ 059\ 81$ nm) into a Siemens D5000 diffractometer with front monochromator. The applied power of the x-ray tube was 35 kV×25 mA and the angular step was 0.005° within the studied 25°–62° range. The quanta acquisition time was 5 s for NTU228,[15] and 20 s for NTU398 and NTU259.

EL and PL emission of thermally annealed samples were studied upon the NTU161 structure. The device was driven with a constant sine wave frequency of 5 kHz and brightness was measured via a Minolta LS110 luminance meter, using the light emitted from an exposed edge on the devices.[13] Upper band gap PL measurements were performed using a 20 Hz pulsed N_2 laser emitting at 337 nm ($E_{\text{excitation}} \sim 3.68$ eV). The peak PL intensities were recorded via an EG&G PARK OMA spectrometer.

III. RESULTS

A. X-ray diffraction analysis

Figure 1 shows selected diffraction angles (27°–32° and 55°–57°) within the XRD patterns of the samples NTU228, NTU398, and NTU259. Here, it should be noted that NTU228 [Fig. 1(a)] and NTU398 [Fig. 1(b)] represent the diffraction patterns of the phosphor and insulating layers individually deposited on Si, and NTU259 represent the diffraction patterns obtained from the ZnS:Mn/Y_2O_3 multilayers deposited on Si as a function of annealing temperature [see Figs. 1(c)–1(g)].

The data in Fig. 1(a) are reported from our previous work,[15] and have been corrected for a quanta acquisition time of 20 s. In Ref. 15, we observed that the ZnS:Mn films exhibit predominantly the zincblende structure with a preferred ⟨111⟩ orientation. In Ref. 15, we also investigated the thermal annealing effects on the crystallinity of ZnS:Mn and concluded that thermal treatments up to 700 °C for 1 h do not induce grain growth or recrystallization of ZnS:Mn when grown onto Si (100) substrates. This conclusion was found to be in agreement with the work from Cattel and Cullis[16] who investigated similar films and substrates. According to our previous work,[15] the observed diffraction peaks in Fig. 1(a) are attributed to the (111) and (311) reflection planes. Recently, a further analysis of these diffraction lines showed that the d spacings of the phosphor lattice monotonically decrease with annealing temperatures from 200 to 700 °C.

The diffraction pattern of the Y_2O_3 thin film deposited on Si (100) is partially shown in Fig. 1(b). The diffraction plane (222) is the only one responsible for significant constructive interference within the investigated diffraction angle range 25°–62°. The calculated diffraction line positions and intensities of Y_2O_3 from the Joint Committee on Powder Diffraction Standards have been presented elsewhere.[17] In its powder form, the normalized theoretical intensities of the three main diffraction planes (222), (400), and (440) are 1, 0.4, and 0.44, respectively, and their positions are at 29.52°, 33.78°, and 48.53°, respectively. In the present work, the (400) and (440) lines do not appear in the diffraction pattern, which implies a radical difference between theoretical and experimental relative intensities. Hence, it is evidenced that the sputtered cubic bixbyite Y_2O_3 structure is preferably oriented in the ⟨111⟩ direction. The approximate position of the diffraction lines observed in Figs. 1(a) and 1(b) are plotted as vertical dashed lines for reference to the following examination.

Figures 1(c)–1(g) represent the XRD patterns of the ZnS:Mn/Y_2O_3 multilayers thermally annealed from 200 to 600 °C for 1 h. First, a qualitative examination of the XRD patterns suggests that the absolute intensity of the ZnS (111) diffraction peak does not change from 200 to 500 °C (~1000 counts), and is increased at 600 °C (~3000 counts). Similarly, the absolute intensity of the Y_2O_3 (222) diffraction peak remains constant from 200 to 400 °C (~1500 counts), and increases from 500 °C (~2000 counts) to 600 °C (>4000 counts). Second, we observe that the diffraction angles $2\theta_{111,\text{ZnS}}$, $2\theta_{222,Y_2O_3}$, and $2\theta_{311,\text{ZnS}}$ shift to higher scattering angles with increasing annealing temperature. In addition, the overall shape modifications of the superposed ZnS (111) and Y_2O_3 (222) diffraction lines suggest that $2\theta_{222,Y_2O_3}$ increases more rapidly than $2\theta_{111,\text{ZnS}}$ [see Figs. 1(e)–1(g)], i.e., modifying the lattice misfit. In order to study these effects further, we deconvoluted the diffraction curves involving both the ZnS (111) and Y_2O_3 (222) lines, using the Laurenzian approximation.

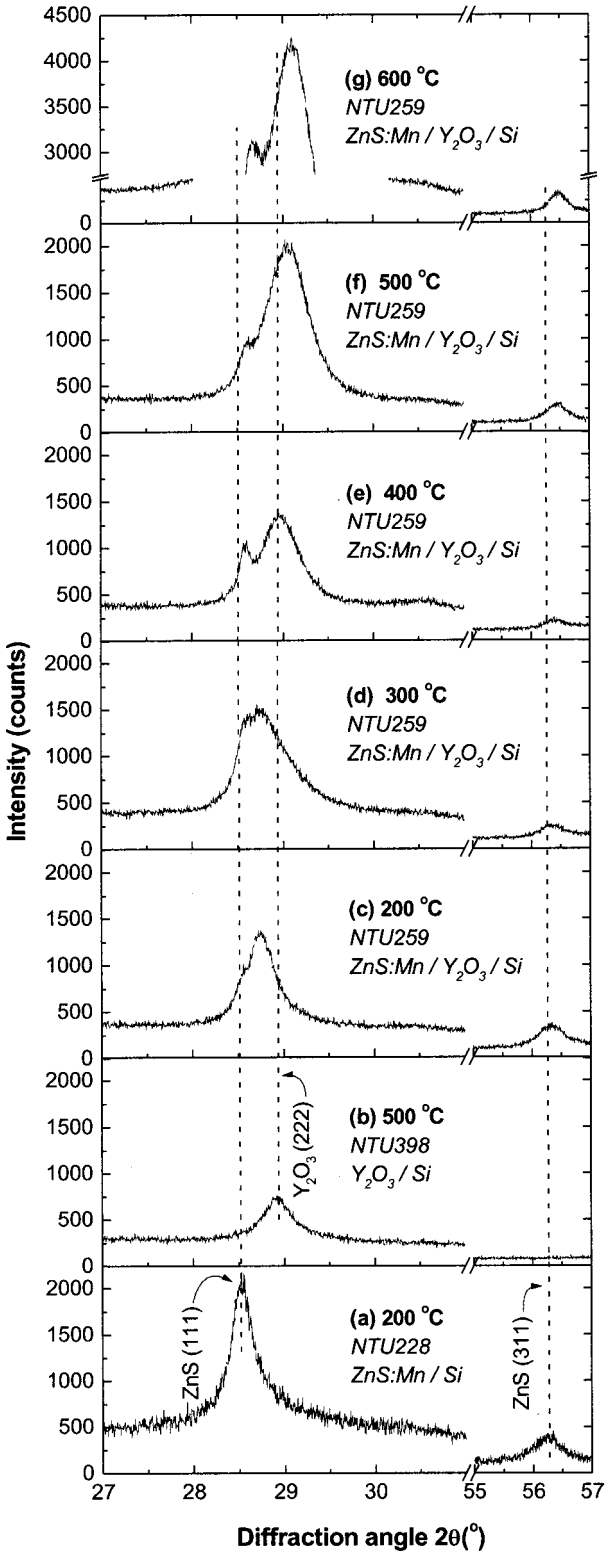

FIG. 1. Partial XRD patterns of thermally annealed thin films as: 800 nm of ZnS:Mn annealed at 200 °C (deposition temperature) (a), 100 nm of Y_2O_3 annealed at 500 °C (b), multilayers of ZnS:Mn (800 nm)/Y_2O_3 (300 nm) annealed at 200 °C (deposition temperature) (c), 300 °C (d), 400 °C (e), 500 °C (f), and 600 °C (g). All thin films and multilayers are deposited onto Si (100) substrates. The vertical dashed lines correspond to the approximate positions of the diffraction lines ZnS (111), Y_2O_3 (222), and ZnS (311) observed in (a) and (b).

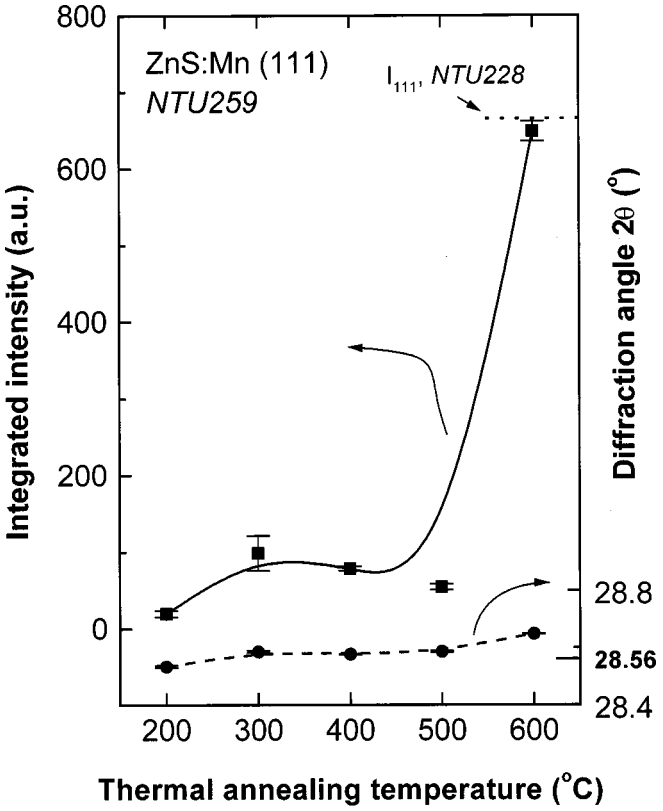

FIG. 2. ZnS (111) diffraction line characteristics as a function of thermal annealing temperature. Data obtained from XRD peak deconvolutions of ZnS:Mn (800 nm)/Y_2O_3 (300 nm) multilayers deposited on Si (100). Curves are generated by computer algorithm and are included for clarity. The diffraction angle value of 28.56 °C corresponds to the calculated (111) diffraction angle of single crystal ZnS. Horizontal dots represent the integrated intensity of a 800 nm thick ZnS:Mn thin film deposited on Si (100) and annealed at temperatures from 200 to 700 °C.

Figures 2 and 3 show the quantitative annealing temperature effects on the integrated intensities and diffraction angles of, respectively, the ZnS (111) and Y_2O_3 (222) lines. The integrated intensity analysis was preferred to maximum intensity since the former is more characteristic of the individual specimens.[18] Here it is confirmed that the integrated intensity increase occurs above 400 and 500 °C, respectively, for the ZnS (111) and Y_2O_3 (222) diffraction lines, and that their diffraction angles increase with increasing annealing temperature. The larger tick marks on the diffraction angle ordinates in Figs. 2 and 3 correspond to the calculated values of, respectively, $2\theta_{111,\mathrm{ZnS}}$ and $2\theta_{222,\mathrm{Y_2O_3}}$, which were determined using the single crystal lattice constants $a_{\mathrm{ZnS}} = 0.541\,02\,\mathrm{nm}$[19] and $a_{\mathrm{Y_2O_3}} = 1.0604\,\mathrm{nm}$[20] [see Eqs. (1) and (2) in Sec. III B]. It is thereby suggested that with increasing annealing temperature, the atomic positions within the sputtered Y_2O_3 crystallites tend to match the perfect crystalline arrangement (Fig. 3), whereas the ZnS:Mn lattice tends to deviate from its undoped single crystal lattice structure (Fig. 2). We note that the summation of the two computed Lorenzian approximations fit very well with the experimental dif-

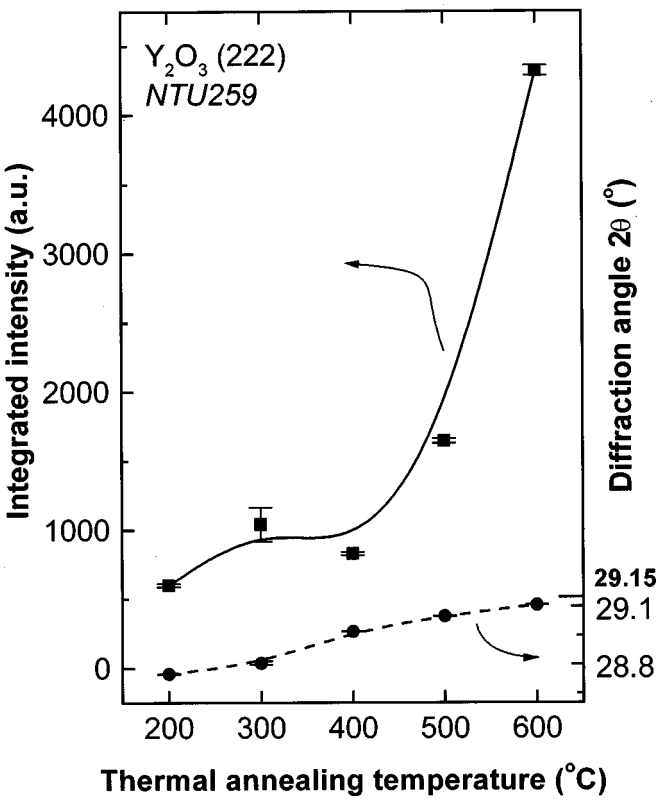

FIG. 3. Y_2O_3(222) diffraction line characteristics as a function of thermal annealing temperature. Data obtained from XRD peak deconvolutions of ZnS:Mn (800 nm)/Y_2O_3 (300 nm) multilayers deposited on Si (100). Curves are generated by computer algorithm and are included for clarity. The diffraction angle value of 29.15 ° corresponds to the calculated (222) diffraction angle of single crystal Y_2O_3.

fraction curves as displayed by the magnitude of the error bars.

Additionally, the horizontal dots in Fig. 2 represent the integrated intensity value of the ZnS (111) diffraction line corresponding to the structure NTU228 [Fig. 1(a)].[15] In Ref. 15, this value was reported to not depend on thermal annealing up to 700 °C. From a direct comparison between NTU228 and NTU259 (Fig. 2), it is obvious that there is a drastic difference in the degree of ⟨111⟩ orientation and in annealing effects when 800 nm of ZnS:Mn are directly deposited on Si or on Si coated with 300 nm of Y_2O_3.

B. Mean lattice constant calculations

The investigated ZnS:Mn and Y_2O_3 lattices both have cubic structures. Hence, the mean lattice constants are calculated from the measured diffraction angles using the Bragg law

$$n\lambda = 2d_{hkl}\sin\theta_{hkl}, \tag{1}$$

and the plane spacing equation for cubic structures

$$(1/d_{hkl})^2 = (h^2+k^2+l^2)/a^2, \tag{2}$$

where n is the order of reflection, λ is the x-ray emission wavelength, d_{hkl} is the distance between adjacent planes of Miller indices hkl, θ_{hkl} is half of the diffraction angle, and a is the lattice constant of the cubic structure.[18] Since there exists a lattice site at the center of the cubic bixbyite Y_2O_3 cell,[21,22] the mean lattice misfits between the insulating and phosphor layers are determined to be

$$1-(a_{Y_2O_3}/2a_{ZnS}). \tag{3}$$

Table II shows the results of the calculated lattice constants and lattice misfits using the mean diffraction angles of the ZnS:Mn (111) and Y_2O_3 (222) lines that are measured from the thermally annealed NTU259 samples (see Figs. 2 and 3). According to our qualitative observations, the lattice misfit between the ZnS:Mn/Y_2O_3 multilayers is affected by the thermal treatment. In Table II, it is shown to remain constant from 200 to 300 °C before increasing sharply from 300 to 500 °C until doubling its initial value.

C. Photoluminescence and electroluminescence analyses

Figure 4 illustrates the PL and EL characteristics of the NTU161 samples thermally annealed from 400 to 700 °C. The plotted PL signals are measured at the maximum of the Mn^{2+} emission spectra and the EL intensities are conventionally measured at an operating potential that is 40 V above threshold voltage.

Both PL and EL intensities are shown to improve with annealing temperatures up to 500 °C. Above 500 °C, the maximum PL intensity increases sharply, whereas the EL brightness saturates. A supplementary PL study of the NTU259 samples exhibits the same behavior.

TABLE II. Results of the phosphor/insulator lattice misfit $1-(a_{Y_2O_3}/2a_{ZnS})$ calculated for the thermally annealed NTU259 samples. $2\theta_{111,ZnS}$ and $2\theta_{222,Y_2O_3}$ are the mean diffraction angles of the ZnS:Mn (111) and Y_2O_3 (222) lines. $d_{111,ZnS}$ and d_{222,Y_2O_3} are their interplanar spacings. $a_{Y_2O_3}$ and a_{ZnS} are the determined lattice constants of the insulator and phosphor layer, respectively.

NTU259		Thermal annealing temperature (°C)				
		200	300	400	500	600
$2\theta_{222,Y_2O_3}$	(°)	28.75	28.80	28.97	29.05	29.10
$2\theta_{111,ZnS}$	(°)	28.53	28.58	28.57	28.58	28.64
d_{222,Y_2O_3}	(nm)	0.310 26	0.309 67	0.307 95	0.307 12	0.306 52
d_{111}, ZnS	(nm)	0.312 56	0.312 00	0.312 10	0.312 00	0.311 34
$a_{Y_2O_3}$	(nm)	1.0747	1.072 72	1.066 77	1.063 89	1.061 81
a_{ZnS}	(nm)	0.541 36	0.540 39	0.540 57	0.540 39	0.539 25
$1-(a_{Y_2O_3}/2a_{ZnS})$	(%)	0.73	0.74	1.32	1.56	1.54

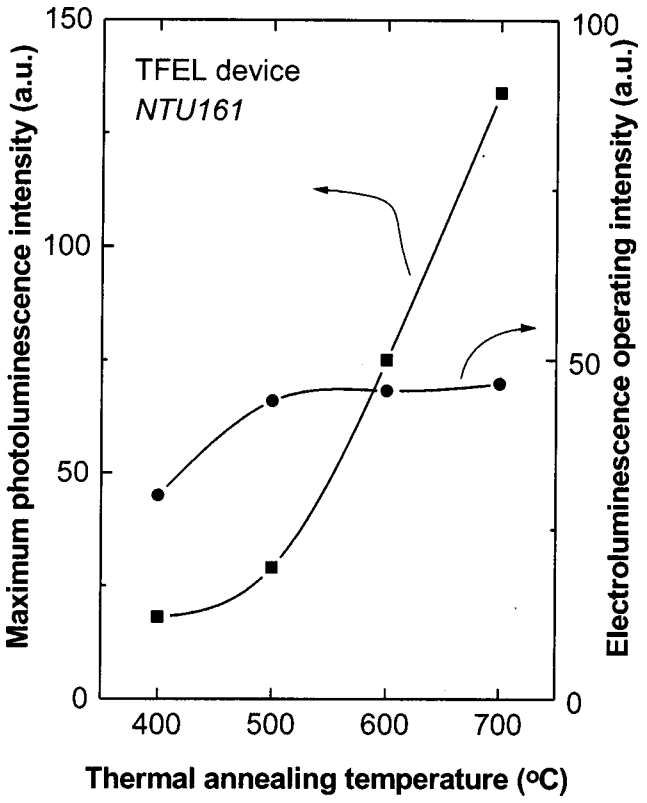

FIG. 4. Maximum photoluminescence intensity and electroluminescence operating intensity as a function of thermal annealing temperature. The ZnS:Mn photoluminescence was excited by a pulsed N_2 laser emitting at an upper band gap wavelength of 337 nm. The TFEL device was driven at a constant sine wave frequency of 5 kHz and the operating intensity was measured at 40 V above threshold voltage.

IV. DISCUSSION

A. Recrystallization effects upon ZnS:Mn and Y_2O_3 thin films at high thermal annealing temperatures

Thermally annealed ZnS:Mn thin films directly deposited on Si did not recrystallize at temperatures up to 700 °C,[15,16] whereas those grown onto Y_2O_3 recrystallize at 600 °C (Fig. 2). Hence, this is direct evidence that the effects of thermal annealing on the crystallinity of our sputtered phosphor layers depend on the substrate used during growth. The integrated intensity of a diffraction line is function of the amount of lattice planes that fulfill the Bragg law. Hence, a direct comparison of the integrated intensities of the ZnS (111) lines (Fig. 2) suggest that the as-grown phosphor layer is less well oriented and of worse crystalline quality when it is deposited on Y_2O_3 (NTU259) and not directly on Si (NTU228). This is not surprising considering the differences between the theoretical lattice misfits of ZnS on Si, and ZnS on Y_2O_3, which are, respectively, ~0.4% and ~2%.[21,23] Moreover, the Si substrate used is monocrystalline, whereas the radio-frequency sputtered Y_2O_3 thin film is highly polycrystalline. It is also sensible to assume that the effectiveness of the thermal annealing process increases with the degree of imperfection of the treated structure. Thus, the observed recrystallization mentioned above might be related to the crystalline quality of the as-grown phosphors, which has been discussed to be substrate dependent. A second factor that may contribute to the recrystallization of the phosphor layer at 600 °C is the recrystallization of the underlying insulator thin film itself. In fact, Y_2O_3 recrystallizes at 500 °C and more significantly at 600 °C (Fig. 3). In Ref. 21, Nakanishi *et al.* reported that the orientation of Y_2O_3 influences that of ZnS. Hence, one could suppose that a reorientation of the Y_2O_3 lattice might favor that of the phosphor layer as well.

A further annealing effect on the ZnS:Mn/Y_2O_3 multilayers (NTU259) is the decrease of their lattice constants (Table II). A possible explanation is that thermal annealing causes an increase in density. From Eqs. (1) and (2), θ_{hkl} increases with $1/a$ for cubic systems, and since the volume of a cubic cell is a^3, the density ρ also increases to $1/a$. Thus, Fig. 3 shows that the sputtered Y_2O_3 structure tends to match the lattice constant and density of its single crystal form, when the annealing temperature increases. Hence, the density increase with increasing treatment temperature may be related to defects and stress removal within the sputtered crystallites. These variations in lattice parameters between the insulating and phosphor layers are directly related to the lattice misfit [see Eq. (3)], which is reported to double at annealing temperatures $>=500$ °C (Table II).

B. Luminescence improvement of ZnS:Mn at high thermal annealing temperatures

From the upper band gap PL results presented in Fig. 4, it is clear that the luminescent quality of the ZnS:Mn thin films is improving with increased thermal annealing temperature up to 700 °C. This is indicative of enhanced luminescent efficiency of the phosphor material, which is the premise behind the standard TFEL annealing process. In this phosphor system, Mn^{2+} ions are radiatively activated by direct substitution on Zn^{2+} lattice sites.[1] Recently, a subband gap PL analysis ($E_{\text{excitation}}<E_{g,\text{ZnS}}$) performed on similar structures did show a linear luminescent efficiency increase in the 200–700 °C range,[24] as opposed to the nonlinear PL behavior seen in Fig. 4. In Ref. 24, we discussed that since we were exciting the second lowest excited states of Mn^{2+} in ZnS, the subband gap PL signals resulting from direct excitation of Mn^{2+} centers are proportional to the number of active Mn centers and not a function of nonradiative recombination paths. Hence, we do not attribute the sharp increase in PL seen in Fig. 4 to a drastic increase in the number of luminescent centers at anneals greater than 500 °C, but rather to the observed recrystallization of the phosphor layer. Indeed, for upper band gap PL analysis, we use excitation energies greater than the ZnS band gap ($E_{g,\text{ZnS}}\sim 3.6$ eV). Hence, the PL efficiency is likely to be dependent on the crystallinity since it involves mechanisms such as electron–hole pair generation and recombination, and energy transfer to luminescent centers.[25] Therefore, we believe that the sharp increase in upper band gap PL above anneals at 500 °C (Fig. 4) is due mainly to recrystallization (Fig. 2), which involves reduced point defects and less nonradiative recombination paths as suggested by Cattel and Cullis.[16]

C. Performance limitation of TFEL devices at high thermal annealing temperatures

The basic excitation mechanisms within ZnS:Mn based TFEL devices can be described as the sequence: (i) tunnel injection of electrons from the phosphor–insulator interface states into the ZnS conduction band; (ii) acceleration to acquire sufficient energy to produce impact excitation of Mn^{2+}; and (iii) luminescent decay of the Mn^{2+} ions.[26] In conventional TFEL devices, the direction of the electric field accelerating the electrons is perpendicular to the film surface, i.e., the cross-sectional direction. Nakanishi and Shimaoka[4] concluded that ZnS:Mn films consisting of a single fiber structure with the [111] axis nearly perpendicular to the substrate, and with good crystallinity in the cross-sectional direction, give the best EL results. They also reported that deterioration in the ZnS (111) orientation increases grain boundaries in the films that decrease the electron mean free path. Accordingly, the improvement in the (111) orientation of our annealed ZnS:Mn phosphor (Fig. 2) will increase the electron mean free path, i.e., reduce the electron energy loss through collisions with stacking defects in the active layer. Moreover, detailed EL decay-time studies by Xian *et al.*[10] have shown that the excitation and radiative efficiencies of TFEL devices are increased when improving the crystallinity of the phosphor. Additionally, in the previous section we suggested that the number of point defects favoring nonradiative recombination are decreased at a thermal treatment of 600 °C, which should further increase the device performance under high anneals.[27]

Here, the EL analysis shows that the TFEL device performance is improved as the annealing temperature is raised from 400 to 500 °C, which is consistent with the reported PL enhancement of ZnS:Mn (Fig. 4). However, from 500 to 700 °C, the EL operating intensity saturates despite the increased number of active Mn^{2+} ions,[24] and the beneficial recrystallization effects upon the excitation, radiative, and electronic properties of the active layer. This lack of significant gain in EL signals was previously suggested to be due to a modification of the interface state distribution, which reduces the density of electrons able to reach optical energies when emitted into the phosphor conduction band.[13] Support for this hypothesis is provided by observed softening effects of the luminance against voltage slope,[13,24] which can be modeled by a modification of the interface state distribution from one dominated by a discrete state (at around 0.9 eV below the conduction band) to one that is a continuum of states.[28] Other research groups who experimentally investigated the thermal annealing effects upon bottom and upper interfaces via polarization measurements arrived at similar conclusions.[11,12]

In this study, we investigated structural modifications within TFEL devices that will further support the above hypotheses. In fact, we have found that the EL saturation occurring at high annealing temperatures corresponds to the maximum ZnS:Mn/Y_2O_3 lattice misfit values reported in Table II. Obviously, these values play an important role in the nature of the electronic interface since lattice misfits are responsible for dislocations, defects, and dangling bonds. Hence, such increase in dangling bonds and deeper defects may generate a more uniform interfacial electron energy distribution and unpin the Fermi level of ZnS:Mn, which has been discussed as being crucial for the generation of so-called hot electrons.[24] In other words, we suggest that the increase in lattice misfit reduces the amount of electrons reaching optical energies, thus reducing the overall performance of TFEL devices.

Since 1997, we have considered the use of pulsed laser annealing as an alternative technique to provide the beneficial luminance gain demonstrated by high temperature annealing, but with minimal effect upon the interface state distribution. Very recently, we reported laser processed TFEL devices exhibiting better display performance than equivalent devices thermally annealed at 450 °C, as demonstrated by the maintenance of a sharp luminance against voltage characteristic with no drop in threshold voltage and a fourfold increase in brightness.[29] Interestingly, the lattice misfit values measured from similarly laser annealed NTU259 structures are smaller than 1.40,[29] which is lower than the values measured from thermally annealed NTU259 structures at 500 °C (Table II). Hence, we inferred that laser annealing can produce the required activation of the thin film phosphors while maintaining a suitable interface state distribution.[29] To conclude, the results of our studies are further evidence that it is important to control the interfacial structure during annealing in order to obtain high-efficiency TFEL devices.

V. CONCLUSIONS

We studied the thermal annealing effects on the crystalline structure of TFEL devices in order to investigate their performance limits resulting from processing at high temperatures. Thus, we systematically investigated the dependence of crystallinity, PL, and EL properties of TFEL structures on thermal annealing temperature. The main results are summarized as follows:

(i) The insulating and phosphor thin films constituting our TFEL devices are preferentially oriented in their ⟨111⟩ direction. The extent of preferred growth in the ⟨111⟩ direction is lower when ZnS:Mn is deposited on the sputtered Y_2O_3 layer than when directly deposited on Si (100).

(ii) Thermally annealing our ZnS:Mn/Y_2O_3 multilayers generates recrystallization of both layers at temperatures of, respectively, 500 and 600 °C. The lattice misfit between both layers increases with annealing and reaches a maximum value at treatment temperatures $>= 500$ °C.

(iii) Upper band gap PL analysis shows that the luminescence properties of the phosphor layer improve sharply above 500 °C. According to a previous subband gap PL study, we infer that the upper band gap PL increase is mainly due to the ZnS:Mn recrystallization.

(iv) The performance of our TFEL device saturates at 500 °C despite the crystalline, luminescent, and electronic transport properties improvements of the active layer. According to an electro-optic model and previous experimental evidence, we suggest that the lattice misfit increase modifies the morphology of the phosphor/insulator boundary and the high field electron transport properties of the device, which

are determined by the interface state distribution.

To conclude, we relate the performance limitations of TFEL devices to interface processing at high annealing temperatures.

ACKNOWLEDGMENTS

The authors, particularly E.A.M., would like to thank E. Fogarassy and M. Robino from PHASE and GONLO Laboratories at Strasbourg, France for providing the means for x-ray diffraction analysis. They also thank M. R. Craven from their research group for his help with the deposition and thermal annealing of the thin films.

[1] P. Rack and P. Holloway, Mater. Sci. Eng., R. **21**, 171 (1998).
[2] T. Inoguchi, M. Takeda, Y. Kakihara, Y. Nakata, and M. Yoshida, SID Dig. **74**, 86 (1974).
[3] C. B. Thomas, R. Stevens, and W. M. Cranton, SID Dig. **96**, 365 (1996).
[4] Y. Nakanishi and G. Shimaoka, J. Vac. Sci. Technol. A **5**, 2092 (1987).
[5] S. Takata, T. Minami, and T. Miyata, Thin Solid Films **193/194**, 481 (1990).
[6] H. Xian, P. Benalloul, C. Barthou, and J. Benoit, Thin Solid Films **248**, 193 (1994).
[7] J. A. Ruffner, R. T. Tuenge, S. Sun, P. D. Grandon, and P. F. Hlava, Thin Solid Films **310**, 123 (1997).
[8] H. Venghaus, D. Theis, H. Oppolzer, and S. Schild, J. Appl. Phys. **53**, 4146 (1982).
[9] T. Matsuoka, J. Kuwata, M. Nishikawa, Y. Fujita, T. Tohida, and A. Abe, Jpn. J. Appl. Phys., Part 1 **27**, 592 (1988).
[10] H. Xian, P. Benalloul, C. Barthou, and J. Benoit, Jpn. J. Appl. Phys., Part 1 **33**, 5801 (1994).
[11] T. Matsuoka, M. Nishikawa, J. Kuwata, Y. Fujita, T. Tohida, and A. Abe, Jpn. J. Appl. Phys., Part 1 **27**, 1430 (1988).
[12] A. Aguilera, S. Bhaskaran, A. Garcia, D. Parker, W. Wu, J. C. McClure, and V. P. Singh, SID Dig. **94**, 452 (1994).
[13] W. M. Cranton, R. Stevens, C. B. Thomas, A. H. Abdullah, and M. R. Craven, Proc. IEE Colloq. Mater. Displays **95**, 7 (1995).
[14] W. M. Cranton, D. M. Spink, R. Stevens, and C. B. Thomas, Thin Solid Films **226**, 156 (1993).
[15] E. A. Mastio, M. Robino, E. Fogarassy, M. R. Craven, W. M. Cranton, and C. B. Thomas, J. Appl. Phys. **86**, 2562 (1999).
[16] A. F. Cattel and A. G. Cullis, Thin Solid Films **92**, 211 (1982).
[17] K. Onisawa, M. Fuyama, K. Tamura, K. Taguchi, T. Nakayama, and Y. A. Ono, J. Appl. Phys. **68**, 719 (1990).
[18] D. B. Cullity, *Elements of X-Ray Diffraction* (Addison-Wesley, Reading, MA, 1978).
[19] J. C. Jamieson and H. H. Demarest, J. Phys. Chem. Solids **41**, 963 (1980).
[20] W. J. Troff and M. E. Thomas, in *Handbook of Optical Constants of Solids II*, edited by E. D. Palik (Academic, New York, 1991), p. 1079.
[21] H. Fukumoto, T. Imura, and Y. Osaka, Appl. Phys. Lett. **55**, 360 (1989).
[22] Y. Nakanishi, Y. Fukuda, Y. Hatanaka, and G. Shimaoka, Appl. Surf. Sci. **48/49**, 297 (1991).
[23] E. A. Mastio, W. M. Cranton, C. B. Thomas, E. Fogarassy, and S. de Unamuno, Appl. Surf. Sci. **139**, 35 (1999).
[24] E. A. Mastio, C. B. Thomas, W. M. Cranton, and E. Fogarassy, Appl. Surf. Sci. **157**, 74 (2000).
[25] R. Scheps, J. Lumin. **42**, 295 (1988).
[26] D. H. Smith, J. Lumin. **23**, 209 (1981).
[27] H. Sasakura, H. Kobayashi, S. Tanaka, J. Mita, T. Tanaka, and H. Nakayama, J. Appl. Phys. **52**, 6901 (1981).
[28] W. M. Cranton, PhD thesis, University of Bradford, 1995.
[29] E. A. Mastio, W. M. Cranton, and C. B. Thomas, J. Appl. Phys. **88**, 1606 (2000).